Chapter 2
Modelling Dielectric Resonators

There are many techniques available for characterising the complex permittivity of microwave dielectric ceramics as functions of temperature and frequency. For materials with modest dielectric loss ($\tan\delta > 10^{-3}$) broadband transmission line measurements can yield the complex permittivity with reasonable accuracy over a wide frequency range. However, for very low loss dielectrics ($\tan\delta < 10^{-4}$) such as the ones studied here, a dielectric resonator technique is required. A dielectric resonator consists of a cylindrical dielectric sample mounted upon a low-loss, low-permittivity support such as quartz or polystyrene, housed within a conducting metallic cylindrical cavity. Microwaves are coupled into the resonator via ports, small loops or probe antennas protruding through the walls of the cavity. The coupling strength is set very low to prevent the resonant frequency of the mode from being perturbed. The resonant frequency and quality factor of a suitable resonant mode can then be measured using a network analyser, either in reflection (one-port) or transmission (two-port). To extract the relative permittivity and loss tangent of a dielectric sample from a microwave measurement or to be able to predict the resonant frequency and quality factor of a resonator, it is necessary to accurately model the electromagnetic fields of resonant modes within dielectric resonator structures. This chapter will apply Maxwell's equations to model the resonant modes supported by cylindrical dielectric resonators using the rigorous analytical technique known as radial mode matching.

2.1 Introduction to Microwave Dielectrics

The dielectric properties of interest to engineers and scientists are the relative permittivity, loss tangent and temperature coefficient of permittivity. They are all, strictly speaking, temperature and frequency dependent, although the relative permittivity is fairly constant over microwave frequencies and can therefore be considered constant to all intensive purposes.

J. Breeze, *Temperature and Frequency Dependence of Complex Permittivity in Metal Oxide Dielectrics: Theory, Modelling and Measurement*, Springer Theses, DOI 10.1007/978-3-319-44547-2_2

Relative Permittivity, ε_r

The real part of the complex permittivity ε_r allows device dimensions to be reduced by a factor of $\sqrt{\varepsilon_r}$ and varies greatly in microwave ceramics, from $\varepsilon_r \approx 4$ for quartz (SiO_2) to $\varepsilon_r > 4000$ for ferroelectrics such as $BaTiO_3$. Almost all single crystal microwave dielectrics with non-cubic crystal structure have anisotropic relative permittivities. For example, a biaxial dielectric would have permittivity tensor:

$$\boldsymbol{\varepsilon} = \begin{bmatrix} \varepsilon_x & 0 & 0 \\ 0 & \varepsilon_y & 0 \\ 0 & 0 & \varepsilon_z \end{bmatrix}.$$

For instance, single crystal rutile TiO_2 is uniaxially anisotropic and has permittivities $\varepsilon_{r,\perp} = 86$ and $\varepsilon_{r,\parallel} = 163$, perpendicular and parallel to the crystal c-axis [1]. Most polycrystalline microwave ceramics have isotropic relative permittivity due to the random orientation of their crystallites, although processing conditions such as temperature gradients can sometimes result in slight anisotropy in the relative permittivity.

Loss Tangent, $\tan\delta$

The ratio of the imaginary and real parts of the complex permittivity, $\tan\delta = \varepsilon''/\varepsilon'$, limits the performance of microwave devices due to absorption of microwave electric field energy. The dielectric quality factor Q_d, an often quoted figure of merit is the reciprocal of the loss tangent, $Q_d = 1/\tan\delta$. The loss tangent is sometimes assumed to vary linearly with frequency, leading to the often quoted Qf factor where the dielectric quality factor Q_d is multiplied by the frequency at which it was measured. Typically, higher permittivity dielectrics have higher dielectric losses. Anisotropic dielectrics such as single crystals will also have tensorial loss tangents with identical symmetry to their relative permittivity tensors. For example, rutile TiO_2 has $\tan\delta_\perp = 1.5 \times 10^{-4}$ and $\tan\delta_\parallel = 1.8 \times 10^{-4}$ for loss tangents perpendicular and parallel to the c-axis at 10 GHz and room temperature.

Temperature Coefficient of Permittivity, τ_ε

This property governs how the centre frequency of a filter or resonant frequency of a dielectric resonator varies with temperature. It is given by the fractional change in the relative permittivity as the temperature varies:

$$\tau_\varepsilon = \frac{1}{\varepsilon_r}\frac{\partial\varepsilon_r}{\partial T}.$$

The temperature coefficient of permittivity (sometimes abbreviated as TCε_r) is often not the property quoted by ceramic manufacturers and engineers. Instead the τ_f or temperature coefficient of frequency (TCf) is reported. This is erroneous since the τ_f is also dependent on the thermal expansion coefficients of the ceramic and the metallic shield, the resonator geometry and resonant mode's electric and magnetic field distributions. Temperature coefficients can be tuned in ceramics by careful

Table 2.1 Typical dielectric properties of some polycrystalline microwave dielectric materials at room temperature [2]

Material	ε_r	$\tau_\varepsilon(\text{ppmK}^{-1})$	$Q_d = 1/\tan\delta$	f(GHz)
$Ba(Mg_{1/3}Ta_{2/3})O_3$	24	0	26,000	10
$Ba(Zn_{1/3}Ta_{2/3})O_3$	30	$-6, \ldots, +6$	12,000	6
$(Zr_{0.8}Sn_{0.2})TiO_4$	38	$-6, \ldots, +6$	8,000	7
$0.7CaTiO_3$-$0.3NdAlO_3$	43	0	7,000	6.7
Al_2O_3	10	+120	100,000	10
TiO_2	100	−900	17,000	3

Table 2.2 Typical dielectric properties of the some single crystal microwave dielectric materials at room temperature [2]. The perpendicular ($\perp$) and parallel ($\parallel$) subscripts refer to components with respect to the crystal c-axis

Material	$\varepsilon_\perp$	$\varepsilon_\parallel$	$\tau_{\varepsilon,\perp}(\text{ppmK}^{-1})$	$\tau_{\varepsilon,\parallel}(\text{ppmK}^{-1})$	$Qf_\perp$	$Qf_\parallel$
SiO_2	4.443	4.644	9	28.7	1,400,000	2,100,000
MgF_2	5.48	4.765	210	–	490,000	220,000
$SrLaAlO_4$	16.85	19.8	50	–	628,000	181,000
Al_2O_3	9.935	11.59	85	121	1,170,000	1,890,000
TiO_2	85.7	163.2	−760	−1200	64,600	56,300

attention to processing, doping and solid solution stoichiometry. For anisotropic dielectrics, the τ_ε also has the same symmetry as the relative permittivity and loss tangent tensors. Again, for rutile TiO_2, values are $\tau_{\varepsilon,\perp} = 760$ ppmK^{-1} and $\tau_{\varepsilon,\parallel} = -1200$ ppmK^{-1} at room temperature. Tables 2.1 and 2.2 show dielectric properties for some common polycrystalline and single crystal microwave dielectric materials.

2.2 Measuring Microwave Dielectric Properties

The measurement of the resonant frequency and quality factor of dielectric resonators as functions of temperature and frequency allows the complex permittivity of a dielectric material to be determined. To transform these measurements into values for the relative permittivity ε_r, loss tangent $\tan\delta$ and temperature coefficient of permittivity τ_ε accurate electromagnetic modelling is required. Furthermore, accurate modelling allows for the optimisation of resonator geometries with respect to losses and spurious modes. The simplest type of apparatus which can be used to measure the dielectric properties of microwave ceramics is the Courtney holder. This device consists of a parallel pair of circular plates which sandwich a small cylindrical ceramic sample. The open sides allow probes or antennae to be inserted in order to excite the resonant mode. The technique was first proposed by

Hakki and Coleman [3] and later analysis of errors and temperature effects were reported by Courtney [4]. Providing that the distance between the plates (the height of the sample) is less than half the free-space wavelength then the electric field of the TE_{011} mode should decay evanescently away from the sample along the radial direction and therefore should not radiate significantly. Kobayashi [5, 6] studied a resonator consisting of a dielectric rod short-circuited at both ends by metal plates and found that the finite diameter of the plates meant that microwave energy could escape by radiation. Furthermore, the transverse magnetic modes (TM) were found to be unsuitable for accurate measurement of the permittivity. The absence of a radial cut-off frequency for TM modes means they have low quality factor due to radiation losses. Small air gaps between the resonator and the plates have considerable effect on the resonant frequency and can lead to large uncertainties in the computed relative permittivity. Ohmic losses induced in the metal plates, due to their proximity to the dielectric sample, limit the measurable $\tan\delta$ since they become the dominant loss mechanism when the dielectric sample has low losses. An obvious loss mitigating step is to separate the dielectric sample from the plates and to use a low-permittivity low-loss dielectric such as quartz or PTFE for support if required. Closing the sides of the resonator will also eliminate radiation losses. DelaBalle et al. [7] numerically studied the case of a dielectric puck within a cavity separated from the cavity walls and Hong [8] studied shielded resonators consisting of pucks placed upon a substrate. Zaki et al. [9] reported highly accurate mode matching results for dielectric samples placed upon low-permittivity supports within cylindrical cavities. Later, Krupka [10], Tobar [11] and Kobayashi [12] reported theoretical and experimental findings for anisotropic dielectrics (mostly single crystals) using highly accurate Rayleigh–Ritz and mode matching methods. They later extended these models to include higher order whispering gallery modes (WGM) which allowed components of the complex permittivity tensor both perpendicular and parallel to the cylindrical axis to be measured [1, 13]. The natural evolution of devices for measuring the complex permittivity of low-loss dielectrics has led to *shielded dielectric resonators* being the most widely employed structures today for measuring the properties of microwave dielectric ceramics.

2.3 Modelling Shielded Dielectric Resonators

Most electromagnetic modelling techniques (and all commercially available software packages), whether they are rigorous or not, take as input the geometry of a structure and the electromagnetic properties of the materials that define it. Typically, the output is the frequency response, or in the case of resonators, the resonant modes of the system. This is important from an engineering point of view when designing devices with an intended frequency response using materials with known properties. From a meteorological point of view this is a hindrance since it is often the electrical properties that are sought given a resonator geometry and measured frequency response. This presents what is known as an *inverse problem* that can be tackled in

various ways. For example, the permittivity of a sample could be found by successive iteration, varying the permittivity in the model until the resonant frequency agrees with measurement. Alternatively, generating a lookup table of values for resonant frequency versus permittivity and interpolating between them could provide reasonably accurate estimates of the permittivity given the resonant frequency. However, both these methods are inherently inefficient since they both require many computation steps. It is desirable to be able to directly calculate the permittivity and loss tangent of a material given a resonant frequency and geometrical description. This is accomplished by modifying existing techniques to solve for permittivity instead of resonant frequency. For the finite-difference time-domain (FDTD) method, the eigenmodes are extracted by spectral analysis of the time-domain response and so this technique cannot be modified. Frequency domain methods such as finite differences or finite elements could be used effectively, but both these techniques have high computational cost if very accurate results are required. The quasi-analytical *mode matching* technique is probably the most accurate method of modelling dielectric resonators, whose accuracy is governed by the number of terms in the truncated series expansion of eigenmode basis functions. The advantage of this technique is that it has very low computational overhead and is very amenable to quickly processing large numbers of data points, which is the case for temperature measurements or optimisation algorithms.

The shielded dielectric resonator as shown in Fig. 2.1, is the most common type of dielectric resonator geometry due to its ease of construction, elimination of radiative losses and reduction of ohmic losses in the conducting shield. It is also the most extensively studied due to its practical application in microwave filters and oscillators as resonant elements. The structure consists of a metal cylindrical cavity, constructed from a high electrical conductivity material such as copper or a silver-plated metal such as brass or aluminium. Inside the cavity is a support structure which is commonly a disk, cylinder or substrate of low-permittivity, low-loss dielectric such as quartz or alumina. The purpose of the support structure is to move the dielectric sample away from the conducting shield to reduce ohmic losses. The dielectric resonator itself is usually a ceramic disk or ring placed on top of the support structure.

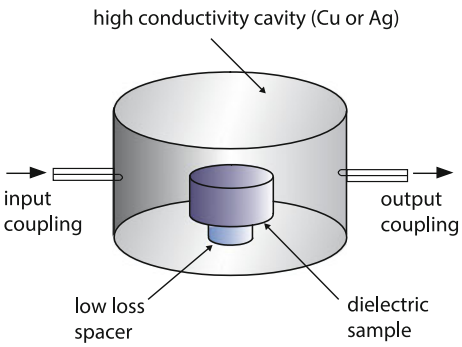

Fig. 2.1 Shielded dielectric resonator

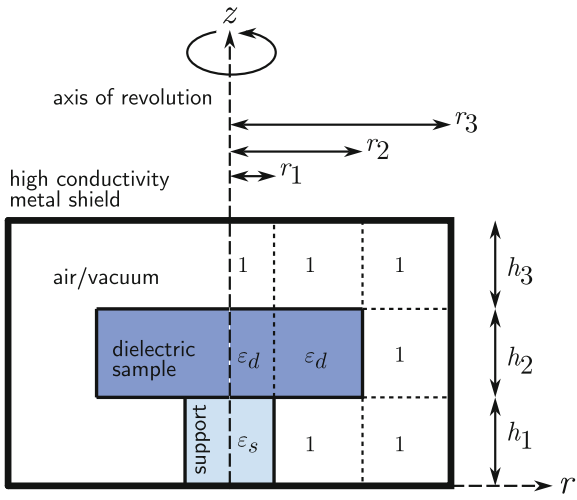

Fig. 2.2 Cross section of dielectric resonator geometry showing how the regions form a 3 × 3 problem space where each piecewise element has an assigned relative permittivity tensor

The structure is symmetrical about the cylindrical axis and so can be considered as a body of revolution with the cross section shown in Fig. 2.2. In the $r - z$ plane, the resonator system can be split up into piecewise regular regions in which the permittivity tensor is homogeneous. The permittivity tensor in each of the nine cells can be represented by a matrix ε_{ijk} where i and j index the layer and radial region of the cell, respectively, and k indexes the component of the permittivity tensor. The electromagnetic fields in each region can be expanded as an infinite series of linear combinations of eigenmodes (basis functions). When the tangential electric and magnetic fields are matched at the interfaces between regions and the boundary conditions on the metallic shield are satisfied, an infinite homogeneous system of linear equations is obtained. The solutions are non-trivial only when the determinant of a characteristic matrix vanishes. Hence, the resonant frequencies or the permittivity can be found by searching for the zeros of the determinant. In practice it is necessary to truncate the series expansion to include a finite number of basis functions. The number of basis functions is increased until an acceptable level of convergence is achieved. For cylindrical symmetric resonators the mode matching method can be approached in two different ways. The axial mode matching method proposed by Zaki [9] first solves a set of eigenvalue problems in the radial direction to obtain eigenvalues which are then used to generate an eigenproblem by matching the fields across layers in the axial direction. Conversely, the radial mode matching method [14] first obtains the eigenvalues for an array of multilayered parallel plate waveguides in the axial direction. Following this step, the fields are matched across region boundaries in the radial direction. Although both radial and axial mode matching techniques have similar accuracy and performance, the radial mode matching technique has an advantage because the first step of the process solves transcendental equations containing only trigonometric functions, whereas the axial technique involves transcendental equations containing Bessel functions.

2.4 Maxwell Equations in Cylindrical Coordinates

To solve the shielded dielectric resonator problem using either the radial or axial mode matching method, one begins with Maxwell's equations in cylindrical coordinates (Fig. 2.3). Maxwell's equations for time harmonic electric **E** and magnetic **H** fields of frequency ω in a linear, homogeneous and source-free medium with anisotropic relative electric permittivity $\tilde{\varepsilon}_r$ and magnetic permeability of free-space, $\mu = \mu_0$ are:

$$\begin{aligned} \nabla \times \mathbf{E} &= -i\omega\mu_0 \mathbf{H}, \\ \nabla \times \mathbf{H} &= +i\omega\varepsilon_0\tilde{\varepsilon}_r \mathbf{E}, \\ \nabla \cdot (\tilde{\varepsilon}_r \mathbf{E}) &= 0, \\ \nabla \cdot \mathbf{H} &= 0. \end{aligned} \tag{2.4.1}$$

The relative permittivity tensor, constrained by the coordinate system to be uniaxial is given by

$$\tilde{\varepsilon}_r = \begin{bmatrix} \varepsilon_t & 0 & 0 \\ 0 & \varepsilon_t & 0 \\ 0 & 0 & \varepsilon_z \end{bmatrix},$$

where ε_t and ε_z are the transverse and longitudinal components with respect to the z-axis. The relative permittivity tensor will be assumed to be purely real, since for useful microwave dielectrics the imaginary part is much smaller than the real part, $\varepsilon'' \ll \varepsilon'$. Equations (2.4.1) can be rearranged in terms of **E** and **H**:

$$\begin{aligned} \mathbf{E} &= -\frac{i}{\omega\varepsilon_0}\tilde{\varepsilon}_r^{-1} \nabla \times \mathbf{H}, \\ \mathbf{H} &= +\frac{i}{\omega\mu_0} \nabla \times \mathbf{E}. \end{aligned} \tag{2.4.2}$$

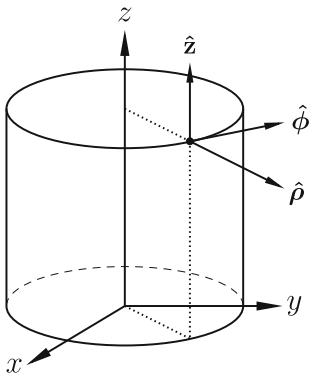

Fig. 2.3 Cylindrical coordinate system

Since the relative permittivity tensor $\tilde{\varepsilon}_r$ is diagonal it is easily inverted and so evaluating the curl operators in cylindrical coordinates provides expressions for the electric and magnetic field components:

$$\begin{aligned}
E_\rho &= -\frac{i}{\omega\varepsilon_0\varepsilon_t}\left\{\frac{1}{\rho}\frac{\partial H_z}{\partial\phi} - \frac{\partial H_\phi}{\partial z}\right\}\\
E_\phi &= -\frac{i}{\omega\varepsilon_0\varepsilon_t}\left\{\frac{\partial H_\rho}{\partial z} - \frac{\partial H_z}{\partial\rho}\right\}\\
E_z &= -\frac{i}{\omega\varepsilon_0\varepsilon_z\rho}\left\{\frac{\partial}{\partial\rho}\left(\rho H_\phi\right) - \frac{\partial H_\rho}{\partial\phi}\right\}\\
H_\rho &= +\frac{i}{\omega\mu_0}\left\{\frac{1}{\rho}\frac{\partial E_z}{\partial\phi} - \frac{\partial E_\phi}{\partial z}\right\}\\
H_\phi &= +\frac{i}{\omega\mu_0}\left\{\frac{\partial E_\rho}{\partial z} - \frac{\partial E_z}{\partial\rho}\right\}\\
H_z &= +\frac{i}{\omega\rho\mu_0}\left\{\frac{\partial}{\partial\rho}\left(\rho E_\phi\right) - \frac{\partial E_\rho}{\partial\phi}\right\}.
\end{aligned} \tag{2.4.3}$$

The equations in ρ and ϕ can be reformulated entirely in terms of the axial field components E_z and H_z by substitution,

$$\begin{aligned}
\left(\frac{\partial^2}{\partial z^2} + k_0^2\varepsilon_t\right)E_\rho &= \frac{\partial^2 E_z}{\partial\rho\partial z} - \frac{i\omega\mu}{\rho}\frac{\partial H_z}{\partial\phi}\\
\left(\frac{\partial^2}{\partial z^2} + k_0^2\varepsilon_t\right)E_\phi &= \frac{1}{\rho}\frac{\partial^2 E_z}{\partial\phi\partial z} + i\omega\mu\frac{\partial H_z}{\partial\rho}\\
\left(\frac{\partial^2}{\partial z^2} + k_0^2\varepsilon_t\right)H_\rho &= \frac{\partial^2 H_z}{\partial\rho\partial z} + \frac{i\omega\varepsilon_0\varepsilon_t}{\rho}\frac{\partial E_z}{\partial\phi}\\
\left(\frac{\partial^2}{\partial z^2} + k_0^2\varepsilon_t\right)H_\phi &= \frac{1}{\rho}\frac{\partial^2 H_z}{\partial\phi\partial z} - i\omega\varepsilon_0\varepsilon_t\frac{\partial E_z}{\partial\rho},
\end{aligned} \tag{2.4.4}$$

where k_0 is the free-space wavenumber. Modes that propagate in the axial z direction can be classified as follows:

- **Transverse electric (TE)**
  These modes have no axial electric field component ($E_z = 0$) and so the electric field is purely transverse (TE). They are designated as h-modes in the literature due to the axial magnetic field component, H_z.
- **Transverse magnetic (TM)**
  These modes have no axial magnetic field component ($H_z = 0$) and so the magnetic field is purely transverse (TM). They are designated as e-modes in the literature due to the axial electric field component, E_z.
- **Hybrid modes (HE/HM)**
  These modes have both electric and magnetic axial field components ($E_z \neq$

0, $H_z \neq 0$). The designation HE (hybrid electric) or HM (hybrid magnetic) depends on which field is dominant in the axial direction.

The next step is to solve Maxwell's equations for the axial field components E_z and H_z. Application of the curl vector operator to both sides of Maxwell's equations (2.4.1) yields

$$\nabla \times \nabla \times \mathbf{E} = -i\omega\mu_0 \nabla \times \mathbf{H} = k_0^2 \tilde{\varepsilon}_r \mathbf{E} \tag{2.4.5}$$

$$\nabla \times \nabla \times \mathbf{H} = +i\omega\varepsilon_0 \nabla \times \tilde{\varepsilon}_r \mathbf{E}. \tag{2.4.6}$$

Applying the double curl vector identity, $\nabla \times \nabla \times \mathbf{A} = \nabla (\nabla \cdot \mathbf{A}) - \nabla^2 \mathbf{A}$, to (2.4.5) gives

$$\nabla^2 \mathbf{E} - \nabla (\nabla \cdot \mathbf{E}) + k_0^2 \tilde{\varepsilon}_r \mathbf{E} = 0. \tag{2.4.7}$$

The divergence of the electric displacement $\mathbf{D}$ is zero, $\nabla \cdot \mathbf{D} = 0$, due to the absence of free charges. For an isotropic dielectric the divergence of the electric field is also zero, because $\nabla \cdot (\varepsilon_r \mathbf{E}) = \varepsilon_r \nabla \cdot \mathbf{E} = 0$. However, for an anisotropic dielectric the divergence of the electric field is not zero since

$$\nabla \cdot (\tilde{\varepsilon}_r \mathbf{E}) = \varepsilon_t \nabla \cdot \mathbf{E} - \varepsilon_t \left(1 - \frac{\varepsilon_z}{\varepsilon_t}\right) \frac{\partial E_z}{\partial z} = 0,$$

resulting in

$$\nabla \cdot \mathbf{E} = \left(1 - \frac{\varepsilon_z}{\varepsilon_t}\right) \frac{\partial E_z}{\partial z}. \tag{2.4.8}$$

Substituting (2.4.8) into (2.4.7) yields

$$\nabla^2 \mathbf{E} - \left(1 - \frac{\varepsilon_z}{\varepsilon_t}\right) \nabla \frac{\partial E_z}{\partial z} + k_0^2 \tilde{\varepsilon}_r \mathbf{E} = 0. \tag{2.4.9}$$

Taking the z component yields the Helmholtz wave equation in E_z:

$$\nabla^2 E_z - \left(1 - \frac{\varepsilon_z}{\varepsilon_t}\right) \frac{\partial^2 E_z}{\partial z^2} + k_0^2 \varepsilon_z E_z = 0. \tag{2.4.10}$$

The Laplacian operator ∇^2, in cylindrical coordinates (see Fig. 2.3) is given by

$$\nabla^2 = \frac{1}{\rho} \frac{\partial}{\partial \rho} \left(\rho \frac{\partial}{\partial \rho}\right) + \frac{1}{\rho^2} \frac{\partial^2}{\partial \phi^2} + \frac{\partial^2}{\partial z^2}. \tag{2.4.11}$$

A solution for E_z of the form

$$E_z(\rho, \phi, z) = R(\rho)\Phi(\phi)Z(z),$$

can be sought by the method of separation of variables. Substituting this in the scalar wave equation (2.4.10) and dividing throughout by $E_z = R(\rho)\Phi(\phi)Z(z)$ produces

$$\frac{1}{\rho R(\rho)}\frac{\partial}{\partial\rho}\left[\rho\frac{\partial R(\rho)}{\partial\rho}\right]+\frac{1}{\rho^2\Phi(\phi)}\frac{\partial^2\Phi(\phi)}{\partial\phi^2}+\frac{1}{Z(z)}\frac{\varepsilon_z}{\varepsilon_t}\frac{\partial^2 Z(z)}{\partial z^2}+k_0^2\varepsilon_z=0. \quad (2.4.12)$$

The third term is independent of both ρ and ϕ and further inspection shows that this term must also be independent of z since the other terms are independent of z and the whole expression sums to zero. The third term must therefore be a coefficient,

$$\frac{1}{Z(z)}\frac{\varepsilon_z}{\varepsilon_t}\frac{\partial^2 Z(z)}{\partial z^2}=-\frac{\varepsilon_z}{\varepsilon_t}\beta^2. \quad (2.4.13)$$

The $-\beta^2$ coefficient is chosen since $Z(z)$ is expected to have an axial variation of the form $e^{i\beta z}$ where β is the propagation constant. Substitution of (2.4.13) into (2.4.12) and multiplying throughout by ρ^2 yields

$$\frac{\rho}{R(\rho)}\frac{\partial}{\partial\rho}\left[\rho\frac{\partial R(\rho)}{\partial\rho}\right]+\frac{1}{\Phi(\phi)}\frac{\partial^2\Phi(\phi)}{\partial\phi^2}+\rho^2\left(k_0^2\varepsilon_z-\frac{\varepsilon_z}{\varepsilon_t}\beta^2\right)=0. \quad (2.4.14)$$

The second term is a function only of ϕ and so the same term independence argument also applies in this case, with m being the azimuthal dependence assuming a variation of the form $e^{im\phi}$, resulting in

$$\frac{1}{\Phi(\phi)}\frac{\partial^2\Phi(\phi)}{\partial\phi^2}=-m^2. \quad (2.4.15)$$

Substitution of (2.4.15) into (2.4.14) and multiplying throughout by $R(\rho)$ gives

$$\rho\frac{\partial}{\partial\rho}\left[\rho\frac{\partial}{\partial\rho}R(\rho)\right]+\left[\lambda^e\rho^2-m^2\right]R(\rho)=0, \quad (2.4.16)$$

where $\lambda^e = k_0^2\varepsilon_z - \frac{\varepsilon_z}{\varepsilon_t}\beta^2$. Notice that (2.4.16) is a partial differential equation in ρ only. We have now separated (2.4.12) into three partial differential equations in $R(\rho)$, $\Phi(\phi)$ and $Z(z)$ (2.4.16), (2.4.15) and (2.4.13). The two equations in z and ϕ are harmonic and therefore have trigonometric solutions. Equation (2.4.16) is a Bessel differential equation of order m and argument $\sqrt{\lambda^e}\rho$. A general solution for $E_z(\rho, \phi, z)$ is therefore given by

$$E_z=\left[A^eJ_m(\xi^e\rho)+B^eY_m(\xi^e\rho)\right]\left[a^e\sin\beta^ez+b^e\cos\beta^ez\right]\left\{\begin{matrix}\cos m\phi\\ \sin m\phi\end{matrix}\right\}, \quad (2.4.17)$$

where $\xi^e = \sqrt{\lambda^e}$ and A^e, B^e, a^e and b^e are coefficients. The e superscript identifies this as an e-mode. J_m and Y_m are Bessel functions of the first and second kinds of

order m [15]. If the Bessel function argument ξ^e is imaginary, then the radial solution will consists of the modified Bessel functions of the first and second kind:

$$I_m(x) = (-i)^m J_m(ix)$$

and

$$K_m(x) = \frac{\pi}{2} i^{m+1} \left[J_m(ix) + iY_m(ix) \right].$$

The radial solution in this case would be

$$R^e(\rho) = A^e I_m(|\xi^e|\rho) + B^e K_m(|\xi^e|\rho).$$

Similarly if the propagation constant is imaginary, the trigonometric functions in the axial eigenfunction are replaced by hyperbolic functions and take the form

$$Z^e(z) = a^e \sinh |\beta^e| z + b^e \cosh |\beta^e| z.$$

Applying the vector identity to the double curl of $\mathbf{H}$, (2.4.6) and noting that the divergence of the magnetic field is zero, $\nabla \cdot \mathbf{H} = 0$, due to the absence of magnetic monopoles, yields:

$$\nabla^2 \mathbf{H} + i\omega\varepsilon_0 \nabla \times \tilde{\varepsilon}_r \mathbf{E} = 0, \tag{2.4.18}$$

and again taking the z component results in the Helmholtz wave equation for H_z:

$$\nabla^2 H_z + k_0^2 \varepsilon_t H_z = 0. \tag{2.4.19}$$

Similar derivation as above for E_z leads to the general solution for H_z:

$$H_z = \left[A^h J_m(\xi^h \rho) + B^h Y_m(\xi^h \rho) \right] \left[a^h \sin \beta^h z + b^h \cos \beta^h z \right] \begin{Bmatrix} \cos m\phi \\ \sin m\phi \end{Bmatrix}, \tag{2.4.20}$$

where $\xi^h = \sqrt{\lambda^h}$ and A^h, B^h, a^h and b^h are coefficients. The separation constant in this case is given by $\lambda^h = k_0^2 \varepsilon_t - (\beta^h)^2$. Remembering that the axial electric and magnetic fields are a superposition of an infinite number of eigenmodes, for any eigenmode p, the radial functions in ρ can be represented by

$$R_p^{e,h}(\rho) = A_p^{e,h} P_p^{e,h}(\rho) + B_p^{e,h} Q_p^{e,h}(\rho), \tag{2.4.21}$$

where

$$P_p^{e,h}(\rho) = \begin{cases} J_m(\xi_p^{e,h}\rho), & \lambda_p^{e,h} > 0 \\ I_m(\xi_p^{e,h}\rho), & \lambda_p^{e,h} < 0 \end{cases} \tag{2.4.22}$$

$$Q_p^{e,h}(\rho) = \begin{cases} Y_m(\xi_p^{e,h}\rho), & \lambda_p^{e,h} > 0 \\ K_m(\xi_p^{e,h}\rho), & \lambda_p^{e,h} < 0 \end{cases} \tag{2.4.23}$$

and $\xi_p^{e,h} = \sqrt{|\lambda_p^{e,h}|}$. The axial eigenfunctions can be represented by

$$Z_p^{e,h}(z) = \begin{cases} a_p^{e,h} \sin \beta_p^{e,h} z + b_p^{e,h} \cos \beta_p^{e,h} z, & (\beta_p^{e,h})^2 > 0 \\ a_p^{e,h} \sinh |\beta_p^{e,h}| z + b_p^{e,h} \cosh |\beta_p^{e,h}| z, & (\beta_p^{e,h})^2 < 0 \end{cases} \tag{2.4.24}$$

and the azimuthal variation by

$$\Phi_m^e(\phi) = \left\{ \begin{array}{c} \cos m\phi \\ \sin m\phi \end{array} \right\} \tag{2.4.25}$$

and

$$\Phi_m^h(\phi) = \left\{ \begin{array}{c} -\sin m\phi \\ \cos m\phi \end{array} \right\}. \tag{2.4.26}$$

Note that $\Phi^{e\prime}(\phi) = m\Phi_m^h(\phi)$ and $\Phi^{h\prime}(\phi) = -m\Phi_m^e(\phi)$, where the prime indicates the derivative with respect to ϕ. General solutions can therefore be expressed in the form:

$$\begin{aligned} E_z &= \sum_p R_p^e(\rho) Z_p^e(z) \Phi_m^e(\phi) \\ H_z &= \sum_p R_p^h(\rho) Z_p^h(z) \Phi_m^h(\phi), \end{aligned}$$

where the summation is over an infinite number of eigenmodes p. The transverse field components are obtained from the axial components using Eqs. (2.4.4),

$$\begin{aligned} E_\rho &= \frac{\varepsilon_z}{\varepsilon_t \lambda^e} \frac{\partial^2 E_z}{\partial \rho \partial z} - \frac{i\omega\mu}{\rho\lambda^h} \frac{\partial H_z}{\partial \phi} \\ E_\phi &= \frac{\varepsilon_z}{\varepsilon_t \lambda^e \rho} \frac{\partial^2 E_z}{\partial \phi \partial z} + \frac{i\omega\mu}{\lambda^h} \frac{\partial H_z}{\partial \rho} \\ H_\rho &= \frac{1}{\lambda^h} \frac{\partial^2 H_z}{\partial \rho \partial z} + \frac{i\omega\varepsilon_0\varepsilon_z}{\rho\lambda^e} \frac{\partial E_z}{\partial \phi} \\ H_\phi &= \frac{1}{\rho\lambda^h} \frac{\partial^2 H_z}{\partial \phi \partial z} - \frac{i\omega\varepsilon_0\varepsilon_z}{\lambda^e} \frac{\partial E_z}{\partial \rho} \end{aligned} \tag{2.4.27}$$

yielding a complete set of field components for each eigenmode p. The field components in cylindrical coordinates can then be written as infinite sums over p:

$$
\begin{aligned}
E_\rho &= \frac{\varepsilon_z}{\varepsilon_t}\sum_p R_p^{e\prime}(\rho)Z_p^{e\prime}(z)\Phi_m^e(\phi) + \frac{im\omega\mu}{\rho}\sum_p R_p^h(\rho)Z_p^h(z)\Phi_m^e(\phi)\\
E_\phi &= \frac{m\varepsilon_z}{\rho\varepsilon_t}\sum_p R_p^e(\rho)Z_p^{e\prime}(z)\Phi_m^h(\phi) + i\omega\mu\sum_p R_p^{h\prime}(\rho)Z_p^h(z)\Phi_m^h(\phi)\\
E_z &= \sum_p \lambda_p^e R_p^e(\rho)Z_p^e(z)\Phi_m^e(\phi)\\
H_\rho &= \frac{im\omega\varepsilon_0\varepsilon_z}{\rho}\sum_p R_p^e(\rho)Z_p^e(z)\Phi_m^h(\phi) + \sum_p R_p^{h\prime}(\rho)Z_p^{h\prime}(z)\Phi_m^h(\phi)\\
H_\phi &= -i\omega\varepsilon_0\varepsilon_z\sum_p R_p^{e\prime}(\rho)Z_p^e(z)\Phi_m^e(\phi) - \frac{m}{\rho}\sum_p R_p^h(\rho)Z_p^{h\prime}(z)\Phi_m^e(\phi)\\
H_z &= \sum_p \lambda_p^h R_p^h(\rho)Z_p^h(z)\Phi_m^h(\phi),
\end{aligned}
\tag{2.4.28}
$$

where the factors $\lambda_p^{e,h}$ have been incorporated into E_z and H_z and primed radial and axial functions represent derivatives with respect to ρ or z. This set of equations allows the field components in any region to be conveniently defined as series expansions of basis functions.

2.5 Multilayer Waveguide Eigenvalues

The multilayer waveguide geometry consists of a parallel plate waveguide partially filled with different layers of dielectric. The eigenvalues λ^e and λ^h can be found for any partial radial region by solving the multilayer waveguide problem shown in Fig. 2.4. Since the axial fields are a superposition of TE and TM modes, the eigenvalues can be found for them independently.

The $\sin m\phi$ and $\cos m\phi$ azimuthal terms can be omitted since they are the same for all layers and radial regions for a given m. Hence, the eigenvalues λ_p^e and λ_p^h are independent of the azimuthal index m. This fact can be used for computational efficiency when searching for solutions for different m indices since the eigenvalues only need to be calculated once for all m. The radial functions can also be omitted since they are layer independent for any partial radial region. For TM modes, where $H_z = 0$, the system of equations for an eigenmode in layer i for a particular partial region is

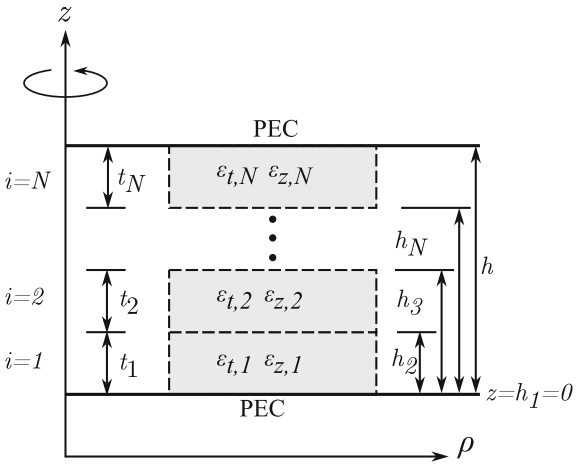

Fig. 2.4 The anisotropic dielectric-loaded parallel plate waveguide. There are N layers of dielectric each with thickness t_i, where $i = 1, 2, \ldots, N$. The multilayer is sandwiched by perfect electric conductors (PEC)

$$
\begin{aligned}
E^e_{\rho,i} &= \frac{\varepsilon_{z,i}}{\varepsilon_{t,i}}\beta^e_i\left[a^e_i\cos\beta^e_i(z-h_i) - b^e_i\sin\beta^e_i(z-h_i)\right]\\
E^e_{\phi,i} &= \frac{\varepsilon_{z,i}}{\varepsilon_{t,i}}\frac{m}{\rho}\beta^e_i\left[a^e_i\cos\beta^e_i(z-h_i) - b^e_i\sin\beta^e_i(z-h_i)\right]\\
E^e_{z,i} &= \lambda^e\left[a^e_i\sin\beta^e_i(z-h_i) + b^e_i\cos\beta^e_i(z-h_i)\right]\\
H^e_{\rho,i} &= \frac{im\omega\varepsilon_0\varepsilon_{z,i}}{\rho}\left[a^e_i\sin\beta^e_i(z-h_i) + b^e_i\cos\beta^e_i(z-h_i)\right]\\
H^e_{\phi,i} &= -i\omega\varepsilon_0\varepsilon_{z,i}\left[a^e_i\sin\beta^e_i(z-h_i) + b^e\cos\beta^e_i(z-h_i)\right]\\
H^e_{z,i} &= 0.
\end{aligned}
\tag{2.5.1}
$$

Similarly, For TE modes, where $E_z = 0$,

$$
\begin{aligned}
E^h_{\rho,i} &= \frac{im\omega\mu}{\rho}\left[a^h_i\sin\beta^h_i(z-h_i) + b^h_i\cos\beta^h_i(z-h_i)\right]\\
E^h_{\phi,i} &= i\omega\mu\left[a^h_i\sin\beta^h_i(z-h_i) + b^h_i\cos\beta^h_i(z-h_i)\right]\\
E^h_{z,i} &= 0\\
H^h_{\rho,i} &= \beta^h_i\left[a^h_i\cos\beta^h_i(z-h_i) - b^h_i\sin\beta^h_i(z-h_i)\right]\\
H^h_{\phi,i} &= -\frac{m}{\rho}\beta^h_i\left[a^h_i\cos\beta^h_i(z-h_i) - b^h_i\sin\beta^h_i(z-h_i)\right]\\
H^h_{z,i} &= \lambda^h\left[a^h_i\sin\beta^h_i(z-h_i) + b^h_i\cos\beta^h_i(z-h_i)\right],
\end{aligned}
$$

where h_i is the height where layer i with thickness t_i begins. The eigenvalues λ^e_p and λ^h_p can be obtained for the multilayer problem by matching the tangential field components at the interfaces between layers and enforcing the boundary conditions on the perfect electric conductors (PEC) at the top and bottom. Matching the tangential

TM and TE fields at the interfaces between layers i and $i+1$ at $z = h_{i+1}$:

$$\begin{aligned} E^e_{\rho,i} &= E^e_{\rho,i+1} \quad E^h_{\rho,i} = E^h_{\rho,i+1} \\ E^e_{\phi,i} &= E^e_{\phi,i+1} \quad E^h_{\phi,i} = E^h_{\phi,i+1} \\ H^e_{\rho,i} &= H^e_{\rho,i+1} \quad H^h_{\rho,i} = H^h_{\rho,i+1} \\ H^e_{\phi,i} &= H^e_{\phi,i+1} \quad H^h_{\phi,i} = H^h_{\phi,i+1}, \end{aligned}$$

results in four equations,

$$\begin{aligned} \frac{\varepsilon_{z,i}}{\varepsilon_{t,i}}\beta^e_i\left(a^e_i\cos\beta^e_i t_i - b^e_i\sin\beta^e_i t_i\right) &= \frac{\varepsilon_{z,i+1}}{\varepsilon_{t,i+1}}\beta^e_{i+1}a^e_{i+1} \\ \varepsilon_{z,i}\left(a^e_i\sin\beta^e_i t_i + b^e\cos\beta^e_i t_i\right) &= \varepsilon_{z,i+1}b^e_{i+1} \\ \left(a^h_i\sin\beta^h_i t_i + b^h_i\cos\beta^h_i t_i\right) &= b^h_{i+1} \\ \beta^h_i\left(a^h_i\cos\beta^h_i t_i - b^h_i\sin\beta^h_i t_i\right) &= \beta^h_{i+1}a^h_{i+1}. \end{aligned}$$

These four equations can be written as a pair of transfer matrix equations relating the coefficients in layer $i+1$ to those in layer i,

$$\begin{bmatrix} a^e_{i+1} \\ b^e_{i+1} \end{bmatrix} = \mathcal{Z}^e_{i,i+1}\begin{bmatrix} a^e_i \\ b^e_i \end{bmatrix},$$
$$\begin{bmatrix} a^h_{i+1} \\ b^h_{i+1} \end{bmatrix} = \mathcal{Z}^h_{i,i+1}\begin{bmatrix} a^h_i \\ b^h_i \end{bmatrix}.$$

The axial transfer matrices $\mathcal{Z}^e_{i,i+1}$ and $\mathcal{Z}^h_{i,i+1}$ are

$$\mathcal{Z}^e_{i,i+1} = \begin{bmatrix} \frac{\varepsilon_{z,i}\varepsilon_{t,i+1}}{\varepsilon_{t,i}\varepsilon_{z,i+1}}\frac{\beta^e_i}{\beta^e_{i+1}}\cos\beta^e_i t_i & -\frac{\varepsilon_{z,i}\varepsilon_{t,i+1}}{\varepsilon_{t,i}\varepsilon_{z,i+1}}\frac{\beta^e_i}{\beta^e_{i+1}}\sin\beta^e_i t_i \\ \frac{\varepsilon_{z,i}}{\varepsilon_{z,i+1}}\sin\beta^e_i t_i & +\frac{\varepsilon_{z,i}}{\varepsilon_{z,i+1}}\cos\beta^e_i t_i \end{bmatrix}$$
$$\mathcal{Z}^h_{i,i+1} = \begin{bmatrix} \frac{\beta^h_i}{\beta^h_{i+1}}\cos\beta^h_i t_i & -\frac{\beta^h_i}{\beta^h_{i+1}}\sin\beta^h_i t_i \\ \sin\beta^h_i t_i & +\cos\beta^h_i t_i \end{bmatrix},$$

where the propagation coefficients $\beta^{(e,h)}_i$ in each layer are calculated from the eigenvalues $\lambda^{(e,h)}$:

$$\beta^e_i = \sqrt{\varepsilon_{t,i}k_0^2 - \frac{\varepsilon_{t,i}}{\varepsilon_{z,i}}\lambda^e}$$
$$\beta^h_i = \sqrt{\varepsilon_{t,i}k_0^2 - \lambda^h}.$$

The PEC boundary condition at the bottom of the multilayer forces the tangential electric field components to be zero,

$$a_1^e = 0$$
$$b_1^h = 0.$$

The coefficients b_1^e and a_1^h can be initially set to unity, then once the eigenvalues have been found, the coefficients a_i^e, b_i^e, a_i^h and b_i^h in all layers are normalised by taking inner products. The coefficients in subsequent layers, $i > 1$, are obtained by applying the transfer matrices to the set of coefficients in the previous layer. Successive multiplication propagates the coefficients for the bottommost layer to the final topmost layer, $i = N$:

$$\begin{bmatrix} a_N^e \\ b_N^e \end{bmatrix} = \prod_{i=1}^{N-1} \mathcal{Z}_{i,i+1}^e \begin{bmatrix} a_1^e \\ b_1^e \end{bmatrix}$$
$$\begin{bmatrix} a_N^h \\ b_N^h \end{bmatrix} = \prod_{i=1}^{N-1} \mathcal{Z}_{i,i+1}^h \begin{bmatrix} a_1^h \\ b_1^h \end{bmatrix}.$$

The eigenvalues are found by searching for solutions which satisfy the boundary conditions on the upper PEC boundary at $z = h$, that the transverse electric field components are zero:

$$E_{\rho,N}^e(h) = 0$$
$$E_{\phi,N}^e(h) = 0$$
$$E_{\rho,N}^h(h) = 0$$
$$E_{\phi,N}^h(h) = 0.$$

These conditions are given by

$$a_N^e \cos \beta_N^e t_N - b_N^e \sin \beta_N^e t_N = 0,$$
$$a_N^h \sin \beta_N^h t_N + b_N^h \cos \beta_N^h t_N = 0. \tag{2.5.2}$$

It can be shown that although there are an infinite number of solutions for the eigenvalues λ_p^e and λ_p^h, there are only a finite number of positive solutions due to the cut-off condition [14]:

$$\lambda_p^{e,h} < k_0^2 \varepsilon_{z,t}^{\max},$$

where the superscript 'max' denotes the highest value of permittivity throughout all the regions in the entire structure. This cut-off condition is used as an upper bound for all eigenvalues. The eigenvalue search is conducted by setting $\lambda^{e,h}$ to a value slightly smaller than $k_0^2 \varepsilon_{z,t}^{\max}$ (setting to exactly this value would mean that $\beta^{e,h}$ would be zero). $\lambda^{e,h}$ is then decreased by small steps until a sign change in Eqs. (2.5.2) is observed. Once a zero has been *bracketed* in this way, the solution can be refined using a root-finding algorithm such as the bisection method [16], Ridders' method [17] or the Brent method [18]. When using the transfer matrix technique, care must be taken to avoid cases where the propagation coefficient $\beta^{e,h}$

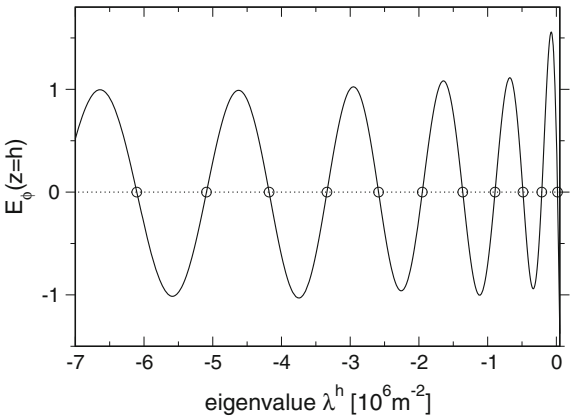

Fig. 2.5 Searching for the *h*-mode (TE) eigenvalues for a 3-layer problem at 10 GHz. The thicknesses of the layers were $t_1 = 4.0$ mm, $t_2 = 5.0$ mm and $t_3 = 6.0$ mm and the transverse permittivities $\varepsilon_{t,1} = 4.3$, $\varepsilon_{t,2} = 10.0$ and $\varepsilon_{t,3} = 1.0$. The circles locate the positions of the eigenvalues

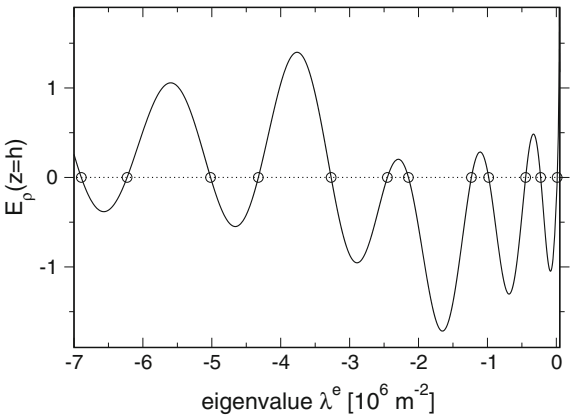

Fig. 2.6 Searching for the *e*-mode (TM) eigenvalues for a 3-layer problem at 10 GHz. The thicknesses of the layers were $t_1 = 4.0$ mm, $t_2 = 5.0$ mm and $t_3 = 6.0$ mm and the transverse permittivities $\varepsilon_{t,1} = 4.3$, $\varepsilon_{t,2} = 10.0$ and $\varepsilon_{t,3} = 1.0$. The circles locate the positions of the eigenvalues

is zero for any layer since this might result in false zeroes. Figures 2.5 and 2.6 show plots of the transverse electric field at the upper PEC for an example three-layer multilayer eigenvalue problem at a frequency of 10 GHz. The first four axial TE and TM eigenmodes are shown in Figs. 2.7 and 2.8. The shaded region shows where the permittivity is highest. Note that E_ϕ is continuous across the dielectric interfaces for the TE case whereas H_ϕ is discontinuous. The derivatives of both are, however, both continuous across the dielectric interfaces.

To be able to use these eigenmodes as basis function for a series expansion of the fields, they are required to be orthogonal and normalised. To investigate this, the previous derivation of the wave equations for the axial fields E_z and H_z, is applied but taking the permittivity tensor to be a function of z. The zero divergence of the displacement, $\nabla \cdot \mathbf{D} = 0$ leads to the following expression for the divergence of the electric field:

$$\nabla \cdot \mathbf{E} = -\frac{1}{\varepsilon_t} \frac{\partial}{\partial z} (\varepsilon_z E_z) + \frac{\partial E_z}{\partial z},$$

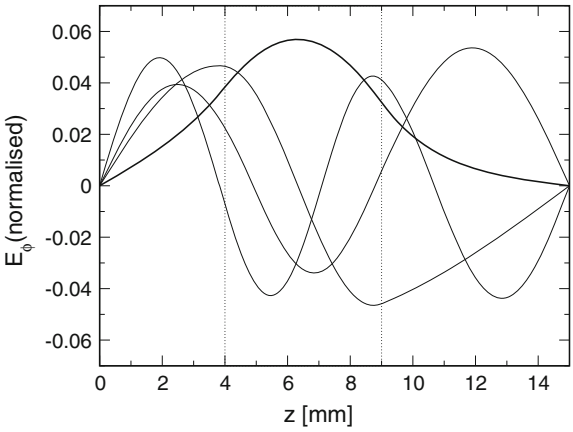

Fig. 2.7 First four axial TE eigenmodes for 3-layer problem at 10 GHz. The thicknesses of the layers were $t_1 = 4.0$ mm, $t_2 = 5.0$ mm and $t_3 = 6.0$ mm and the transverse permittivities $\varepsilon_{t,1} = 4.3$, $\varepsilon_{t,2} = 10.0$ and $\varepsilon_{t,3} = 1.0$

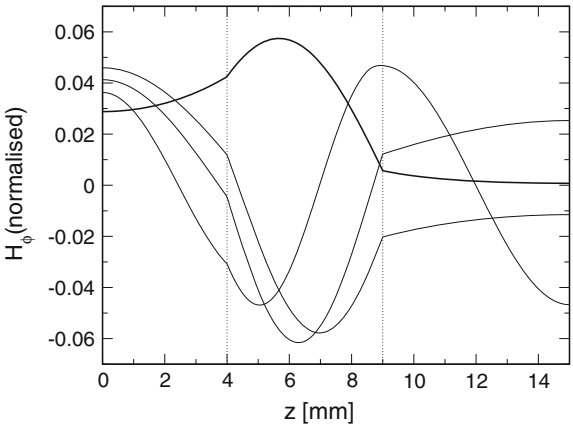

Fig. 2.8 First four axial TM eigenmodes for 3-layer problem at 10 GHz. The thicknesses of the layers were $t_1 = 4.0$ mm, $t_2 = 5.0$ mm and $t_3 = 6.0$ mm and the transverse permittivities $\varepsilon_{t,1} = 4.3$, $\varepsilon_{t,2} = 10.0$ and $\varepsilon_{t,3} = 1.0$

and so the partial differential equation for E_z is modified slightly:

$$\nabla^2 E_z + \frac{\partial}{\partial z}\left[\frac{1}{\varepsilon_t}\frac{\partial}{\partial z}(\varepsilon_z E_z)\right] - \frac{\partial^2 E_z}{\partial z^2} + k_0^2 \tilde{\varepsilon}_r \mathbf{E} = 0.$$

Substituting $E_z = R(\rho)\Phi(\phi)Z(z)$, dividing throughout by E_z and equating the term in z to the same coefficient in Eq. (2.4.13), namely $-\beta^2 \varepsilon_t/\varepsilon_t$, produces a Sturm–Liouville [15] partial differential equation:

$$\frac{\partial}{\partial z}\left\{\frac{1}{\varepsilon_t}\frac{\partial}{\partial z}\left[\varepsilon_z Z(z)\right]\right\} + \left(k_0^2 - \frac{\lambda_e}{\varepsilon_z}\right)\left[\varepsilon_z Z(z)\right] = 0.$$

The weighted inner product of two axial TM eigenmodes spanning the height h of a resonator is then:

$$\int_0^h \varepsilon_z Z_p^e(z) Z_q^e(z) dz = \delta_{pq}$$

where δ_{pq} is the Kronecker delta. The inner product for TE eigenmodes can be found similarly, yet is not weighted:

$$\int_0^h Z_p^h(z) Z_q^h(z) dz = \delta_{pq}.$$

The orthonormality of the axial eigenmodes whilst not entirely crucial for a field expansion to be possible, nevertheless make the matching of field at the radial interfaces easier, since the field series can be *tested* by appropriate eigenmodes resulting in diagonal matrices which are easier to invert.

2.6 The Radial Mode Matching Method

Once a prescribed number of eigenvalues λ_p^{ej} and λ_p^{hj} and their associated eigenmodes have been found for the multilayer parallel waveguide for each radial region j, it is necessary to execute the next step which is matching the transverse fields at the interfaces between radial regions. The equations for the transverse fields E_ϕ, H_ϕ, E_z and H_z, (omitting ϕ dependence) (Eq. 2.4.28) are:

$$\begin{aligned}
E_\phi(\rho, z) &= \frac{m\varepsilon_z}{\rho\varepsilon_t} \sum_p R_p^e(\rho) Z_p^{e\prime}(z) + i\omega\mu \sum_p R_p^{h\prime}(\rho) Z_p^h(z) \\
E_z(\rho, z) &= \sum_p \lambda_p^e R_p^e(\rho) Z_p^e(z) \\
H_\phi(\rho, z) &= -i\omega\varepsilon_0\varepsilon_z \sum_p R_p^{e\prime}(\rho) Z_p^e(z) - \frac{m}{\rho} \sum_p R_p^h(\rho) Z_p^{h\prime}(z) \\
H_z(\rho, z) &= \sum_p \lambda_p^h R_p^h(\rho) Z_p^h(z).
\end{aligned} \tag{2.6.1}$$

Recalling that the radial functions are given by

$$R_p^{e,h}(\rho) = A_p^{e,h} P_p^{e,h}(\rho) + B_p^{e,h} Q_p^{e,h}(\rho), \tag{2.6.2}$$

and matching the tangential fields on the boundaries between regions $j+1$ and j at radius ρ:

$$\begin{aligned}
E_\phi^{j+1}(\rho) &= E_\phi^j(\rho) \\
E_z^{j+1}(\rho) &= E_z^j(\rho) \\
H_\phi^{j+1}(\rho) &= H_\phi^j(\rho) \\
H_z^{j+1}(\rho) &= H_z^j(\rho),
\end{aligned}$$

results in the following set of four equations (where the ρ and z dependence of the radial and axial eigenfunctions is assumed):

$$\begin{aligned}
&\frac{m\varepsilon_z}{\rho\varepsilon_t}\sum_p P^e_{p,j+1}Z^{e\prime}_{p,j+1}A^e_{p,j+1}+\frac{m\varepsilon_z}{\rho\varepsilon_t}\sum_p Q^e_{p,j+1}Z^{e\prime}_{p,j+1}B^e_{p,j+1}\\
&\qquad+i\omega\mu\sum_p P^{h\prime}_{p,j+1}Z^h_{p,j+1}A^h_{p,j+1}+i\omega\mu\sum_p Q^{h\prime}_{p,j+1}Z^h_{p,j+1}B^h_{p,j+1}=\\
&\frac{m\varepsilon_z}{\rho\varepsilon_t}\sum_p P^e_{p,j}Z^{e\prime}_{p,j}A^e_{p,j}+\frac{m\varepsilon_z}{\rho\varepsilon_t}\sum_p Q^e_{p,j}Z^{e\prime}_{p,j}B^e_{p,j}+i\omega\mu\sum_p P^{h\prime}_{p,j}Z^h_{p,j}A^h_{p,j}+i\omega\mu\sum_p Q^{h\prime}_{p,j}Z^h_{p,j}B^h_{p,j}\\
&\qquad\sum_p\lambda^e_{p,j+1}P^e_{p,j+1}Z^e_{p,j+1}A^e_{p,j+1}+\sum_p\lambda^e_{p,j+1}Q^e_{p,j+1}Z^e_{p,j+1}B^e_{p,j+1}=\\
&\qquad\qquad\sum_p\lambda^e_{p,j}P^e_{p,j}Z^e_{p,j}A^e_{p,j}+\sum_p\lambda^e_{p,j}Q^e_{p,j}Z^e_{p,j}B^e_{p,j}\\
&\qquad i\omega\varepsilon_0\varepsilon_z\sum_p P^{e\prime}_{p,j+1}Z^e_{p,j+1}A^e_{p,j+1}+i\omega\varepsilon_0\varepsilon_z\sum_p Q^{e\prime}_{p,j+1}Z^e_{p,j+1}B^e_{p,j+1}\\
&\qquad+\frac{m}{\rho}\sum_p P^h_{p,j+1}Z^{h\prime}_{p,j+1}A^h_{p,j+1}+\frac{m}{\rho}\sum_p Q^h_{p,j+1}Z^{h\prime}_{p,j+1}B^h_{p,j+1}=\\
&\qquad\qquad i\omega\varepsilon_0\varepsilon_z\sum_p P^{e\prime}_{p,j}Z^e_{p,j}A^e_{p,j}+i\omega\varepsilon_0\varepsilon_z\sum_p Q^{e\prime}_{p,j}Z^e_{p,j}B^e_{p,j}\\
&\qquad\qquad+\frac{m}{\rho}\sum_p P^h_{p,j}Z^{h\prime}_{p,j}A^h_{p,j}+\frac{m}{\rho}\sum_p Q^h_{p,j}Z^{h\prime}_{p,j}B^h_{p,j}\\
&\qquad\sum_p\lambda^h_{p,j+1}P^h_{p,j+1}Z^h_{p,j+1}A^h_{p,j+1}+\sum_p\lambda^h_{p,j+1}Q^h_{p,j+1}Z^h_{p,j+1}B^h_{p,j+1}=\\
&\qquad\qquad\sum_p\lambda^h_{p,j}P^h_{p,j}Z^h_{p,j}A^h_{p,j}+\sum_p\lambda^h_{p,j}Q^h_{p,j}Z^h_{p,j}B^h_{p,j}\,.
\end{aligned}$$

Multiplying each equation with appropriate axial eigenmodes (labelled q) as testing functions, integrating from $z=0$ to $z=h$ and rearranging produces the following block matrix equation relating the coefficients in region $j+1$ with those in region j,

$$\begin{bmatrix} A^e_{j+1}\\ B^e_{j+1}\\ A^h_{j+1}\\ B^h_{j+1}\end{bmatrix}=\underbrace{\left[\begin{array}{cc|cc} C & D & 0 & 0\\ G & H & I & J\\ \hline O & P & Q & R\\ 0 & 0 & W & X\end{array}\right]^{-1}\left[\begin{array}{cc|cc} E & F & 0 & 0\\ K & L & M & N\\ \hline S & T & U & V\\ 0 & 0 & Y & Z\end{array}\right]}_{\mathcal{R}_{j,j+1}(\rho)}\begin{bmatrix} A^e_j\\ B^e_j\\ A^h_j\\ B^h_j\end{bmatrix}. \tag{2.6.3}$$

Analogous to the axial eigenproblem, this introduces the radial transfer matrix $\mathcal{R}_{j,j+1}(\rho)$ which relates the coefficients A^e_j, B^e_j, A^h_j and B^h_j in region j to those in region $j+1$. The matrices represented by capital letters (with rows p and columns q) are

$$
\begin{aligned}
C &= \lambda^e_{p,j+1} P^e_{p,j+1} \delta_{pq} \\
D &= \lambda^e_{p,j+1} Q^e_{p,j+1} \delta_{pq} \\
E &= \lambda^e_{p,j} P^e_{p,j} \left\langle \varepsilon_z Z^e_{q,j+1}, Z^e_{p,j} \right\rangle \\
F &= \lambda^e_{p,j} Q^e_{p,j} \left\langle \varepsilon_z Z^e_{q,j+1}, Z^e_{p,j} \right\rangle \\
G &= i\omega\varepsilon_0 P^{e\prime}_{p,j+1} \delta_{pq} \\
H &= i\omega\varepsilon_0 Q^{e\prime}_{p,j+1} \delta_{pq} \\
I &= \frac{m}{\rho} P^h_{p,j+1} \left\langle Z^e_{q,j+1}, Z^{h\prime}_{p,j+1} \right\rangle \\
J &= \frac{m}{\rho} Q^h_{p,j+1} \left\langle Z^e_{q,j+1}, Z^{h\prime}_{p,j+1} \right\rangle \\
K &= i\omega\varepsilon_0 P^{e\prime}_{p,j} \left\langle Z^e_{q,j+1}, \varepsilon_z Z^e_{p,j} \right\rangle \\
L &= i\omega\varepsilon_0 Q^{e\prime}_{p,j} \left\langle Z^e_{q,j+1}, \varepsilon_z Z^e_{p,j} \right\rangle \\
M &= \frac{m}{\rho} P^h_{p,j} \left\langle Z^e_{q,j+1}, Z^{h\prime}_{p,j} \right\rangle \\
N &= \frac{m}{\rho} Q^h_{p,j} \left\langle Z^e_{q,j+1}, Z^{h\prime}_{p,j} \right\rangle \\
O &= \frac{m}{\rho} P^e_{p,j+1} \left\langle Z^h_{q,j+1}, \frac{\varepsilon_z}{\varepsilon_t} Z^{e\prime}_{p,j+1} \right\rangle \\
P &= \frac{m}{\rho} Q^e_{p,j+1} \left\langle Z^h_{q,j+1}, \frac{\varepsilon_z}{\varepsilon_t} Z^{e\prime}_{p,j+1} \right\rangle \\
Q &= i\omega\mu P^{h\prime}_{p,j+1} \delta_{pq} \\
R &= i\omega\mu Q^{h\prime}_{p,j+1} \delta_{pq} \\
S &= \frac{m}{\rho} P^e_{p,j} \left\langle Z^e_{q,j+1}, \frac{\varepsilon_z}{\varepsilon_t} Z^{e\prime}_{p,j} \right\rangle \\
T &= \frac{m}{\rho} Q^e_{p,j} \left\langle Z^e_{q,j+1}, \frac{\varepsilon_z}{\varepsilon_t} Z^{e\prime}_{p,j} \right\rangle \\
U &= i\omega\mu P^{h\prime}_{p,j} \left\langle Z^h_{q,j+1}, Z^h_{p,j} \right\rangle \\
V &= i\omega\mu Q^{h\prime}_{p,j} \left\langle Z^h_{q,j+1}, Z^h_{p,j} \right\rangle \\
W &= \lambda^h_{p,j+1} P^h_{p,j+1} \delta_{pq} \\
X &= \lambda^h_{p,j+1} Q^h_{p,j+1} \delta_{pq} \\
Y &= \lambda^h_{p,j} P^h_{p,j} \left\langle Z^h_{q,j+1}, Z^h_{p,j} \right\rangle \\
Z &= \lambda^h_{p,j} Q^h_{p,j} \left\langle Z^h_{q,j+1}, Z^h_{p,j} \right\rangle .
\end{aligned}
$$

where the terms inside angular brackets are coupling integrals between axial eigenfunctions in regions j and $j+1$, for example.

$$\int_0^h Z^h_{p,j}(z) Z^h_{q,j+1}(z) dz = \left\langle Z^h_{q,j+1}, Z^h_{p,j} \right\rangle .$$

If the azimuthal index is zero, $m = 0$, then the transverse TE_0 and TM_0 modes become axisymmetric and decoupled, having only electric or magnetic azimuthal field components. The matrices I, J, M, N, O, P, S and T containing terms in m then become zero and the radial transfer matrix $\mathcal{R}^{m=0}$ assumes a much simpler form:

$$\mathcal{R}^{m=0}_{j,j+1}(\rho) = \left[\begin{array}{cc|cc} C & D & 0 & 0 \\ G & H & 0 & 0 \\ \hline 0 & 0 & Q & R \\ 0 & 0 & W & X \end{array}\right]^{-1} \left[\begin{array}{cc|cc} E & F & 0 & 0 \\ K & L & 0 & 0 \\ \hline 0 & 0 & U & V \\ 0 & 0 & Y & Z \end{array}\right] . \tag{2.6.4}$$

The TE and TM mode coefficients A^h_j, B^h_j and A^e_j, B^e_j are become independent of one another and can be solved independently. The radial transfer matrix $\mathcal{R}^{m=0}_{j,j+1}(\rho)$ then splits into two smaller transfer matrices for the axisymmetric ($m = 0$) TE and TM modes:

$$\mathcal{R}^{e,m=0}_{j,j+1}(\rho) = \left[\begin{array}{cc} C & D \\ G & H \end{array}\right]^{-1} \left[\begin{array}{cc} E & F \\ K & L \end{array}\right], \tag{2.6.5}$$

$$\mathcal{R}^{h,m=0}_{j,j+1}(\rho) = \left[\begin{array}{cc} Q & R \\ W & X \end{array}\right]^{-1} \left[\begin{array}{cc} U & V \\ Y & Z \end{array}\right]. \tag{2.6.6}$$

In a similar way to how the axial eigenproblem was solved earlier by cascading transfer matrices, the modal coefficients A^e_j, B^e_j, A^h_j and B^h_j of the outer region $j = N_\rho$, can be calculated by successive application of radial transfer matrices to the coefficients in the innermost region $j = 1$:

$$\left[\begin{array}{c} A^e_{N_\rho} \\ B^e_{N_\rho} \\ \hline A^h_{N_\rho} \\ B^h_{N_\rho} \end{array}\right] = \prod_{j=1}^{N\rho-1} \mathcal{R}_{j,j+1}(\rho_{j+1}) \left[\begin{array}{c} A^e_1 \\ B^e_1 \\ \hline A^h_1 \\ B^h_1 \end{array}\right] . \tag{2.6.7}$$

Due to singularities at the origin $\rho = 0$ being unphysical, the set of coefficients B^e_1 and B^h_1 of the Bessel functions of the second kind in the first radial partial region can be set to zero. Similarly to the axial eigenproblem, since the eigenmodes are orthonormal, the set of coefficients A^e_1 and A^h_1 can be initially be set to unity and then renormalised once a solution has been found. The modal coefficients A^e_j, B^e_j, A^h_j and B^h_j for the outer region are used to enforce the boundary condition on the outer radial cavity wall ($\rho = a$), namely that the tangential electric field is zero:

$$E_\phi(a) = \frac{m\varepsilon_z}{a\varepsilon_t}\sum_p A_p^e P_p^e(a) Z_p^{e\prime}(z) + i\omega\mu \sum_p A_p^h P_p^{h\prime}(a) Z_p^h(z)$$
$$+ \frac{m\varepsilon_z}{a\varepsilon_t}\sum_p B^e Q_p^e(a) Z_p^{e\prime}(z) + i\omega\mu \sum_p B_p^h Q_p^{h\prime}(a) Z_p^h(z) = 0$$
$$E_z(a) = \sum_p \lambda_p^e A_p^e P_p^e(a) Z_p^e(z) + \sum_p \lambda_p^e B_p^e Q_p^e(a) Z_p^e(z) = 0 \tag{2.6.8}$$

Similar to the previously applied method of using testing functions, multiplying Eq. (2.6.8) by the appropriate testing function $\varepsilon_z Z_q^e(z)$ and integrating from $z = 0$ to $z = h$, results in the following matrix equation for e-modes:

$$\left[\begin{array}{ccc|ccc} P_1^e(a) & & & Q_1^e(a) & & \\ & \ddots & & & \ddots & \\ & & P_N^e(a) & & & Q_N^e(a) \end{array}\right] \left[\begin{array}{c} A_1^e \\ \vdots \\ A_N^e \\ \hline B_1^e \\ \vdots \\ B_N^e \end{array}\right] = 0, \tag{2.6.9}$$

where for each row $i = 1 \ldots N$, corresponds to each eigenmode in the expansion

$$A_i^e P_i^e(a) + B_i^e Q_i^e(a) = 0.$$

Substituting these into Eq. (2.6.8) and simplifying yields

$$E_\phi(a) = \sum_p A_p^h P_p^{h\prime}(a) Z_p^h(z) + \sum_p B_p^h Q_p^{h\prime}(a) Z_p^h(z) = 0, \tag{2.6.10}$$

which upon multiplication by testing functions $Z_q^h(z)$ and integrating from $z = 0$ to $z = h$ yields another matrix equation for the coefficients of h-modes, A^h and B^h:

$$\left[\begin{array}{ccc|ccc} P_1^{h\prime}(a) & & & Q_1^{h\prime}(a) & & \\ & \ddots & & & \ddots & \\ & & P_N^{h\prime}(a) & & & Q_N^{h\prime}(a) \end{array}\right] \left[\begin{array}{c} A_1^h \\ \vdots \\ A_N^h \\ \hline B_1^h \\ \vdots \\ B_N^h \end{array}\right] = 0, \tag{2.6.11}$$

where for each row $i = 1 \ldots N$, corresponds to each eigenmode in the expansion,

$$A_i^h P_i^{h\prime}(a) + B_i^h Q_i^{h\prime}(a) = 0.$$

These two sets of boundary conditions together form a matrix which when multiplied by the transfer matrix $\mathcal{R}_{1,N_\rho}$, relates the coefficients in the last outer radial region N_ρ to those in the first inner radial region:

$$\mathcal{R}_{1,N_\rho} = \prod_{j=1}^{N\rho-1} \mathcal{R}_{j,j+1}(\rho_{j+1}). \tag{2.6.12}$$

Recalling that the B_1^e and B_1^h coefficients in the innermost region are zero, allows a characteristic matrix equation to be formed:

$$\mathcal{T} \begin{bmatrix} A_{N_\rho}^e \\ \hline A_{N_\rho}^h \end{bmatrix} = 0. \tag{2.6.13}$$

Non-trivial solutions occur when the determinants of the characteristic matrix $\mathcal{T}$ are zero. The zeros of the determinant, $\det(\mathcal{T})$ are found in the same way as the eigenvalues for the multilayer waveguide, bracketing followed by Ridders' method. Once a solution is found the radial coefficients A^e, B^e, A^h and B^h are normalised using the orthonormal properties of Bessel functions.

2.7 Calculating Resonator Losses

Once a solution for a particular mode has been found, the losses in the resonator can be calculated by volume integration of the electric and magnetic field energy densities for all regions and surface integration of the tangential magnetic field on conducting surfaces. The *unloaded* quality factor Q for a resonator is the ratio of total stored energy to the power dissipated per oscillatory cycle with period $T = \frac{2\pi}{\omega}$,

$$Q = \frac{\omega U}{W_d + W_c}$$

where U is the total stored energy in the resonator and W_d and W_c are dielectric and conductor losses. The reciprocal of this, which can be thought of as total loss, is the sum of the dielectric and conductor losses:

$$\frac{1}{Q} = \frac{1}{Q_d} + \frac{1}{Q_c} = \frac{W_d}{\omega U} + \frac{W_c}{\omega U}.$$

Representing the total loss as a sum of individual losses from either dielectric or conductive sources allows these parts to be calculated separately and is also informative when designing resonators, allowing the largest contributors to the total loss to be identified and reduced by attention to geometry or material properties.

Dielectric Losses

The total internal electromagnetic energy in an anisotropic dielectric can be found by integrating the modulus of the electric energy density over the volume of the resonator,

$$U = \sum_p U_p = \frac{1}{2} \sum_p \int_{V_p} \varepsilon_p' \mathbf{E} \cdot \mathbf{E}^* \, \mathrm{d}V,$$

where the summation is over all partial regions p comprising the resonator and U_p is the total internal electromagnetic energy in partial region p. The complex electric permittivity tensor for region p is $\boldsymbol{\varepsilon}_p = \boldsymbol{\varepsilon}_p' + i\boldsymbol{\varepsilon}_p''$ or

$$\boldsymbol{\varepsilon}_p = \varepsilon_0 \begin{bmatrix} \varepsilon_{t,p} & 0 & 0 \\ 0 & \varepsilon_{t,p} & 0 \\ 0 & 0 & \varepsilon_{z,p} \end{bmatrix}.$$

Similarly, the dielectric dissipation for a region p is found by integrating the imaginary part of the electric energy density over the volume V_p

$$W_{d,p} = \frac{\omega}{2} \sum_p \int_{V_p} \boldsymbol{\varepsilon}_p'' \mathbf{E} \cdot \mathbf{E}^* \, \mathrm{d}V.$$

The loss tangent, $\tan\delta = \varepsilon''/\varepsilon'$, the ratio of imaginary and real parts of the complex permittivity, allows the dielectric loss for region p to be written

$$\frac{1}{Q_{d,p}} = \frac{W_{d,p}}{\omega U} = \frac{\tan\delta_p U_p}{U} = P_{d,p} \tan\delta_p,$$

which introduces the electric filling factor for a region p, defined

$$P_{d,p} = \frac{U_p}{U}.$$

The electric filling factor $P_{d,p}$ is the fraction of the total electric energy in a resonator residing within region p. Due to the scale invariance of Maxwell's equations, the electric filling factors are also frequency invariant. To calculate the integrals, the expressions developed earlier for the electric fields can be used:

$$E_\rho = \sum_n R_n^{e\prime}(\rho) Z_n^{e\prime}(z) \Phi_m^e(\phi) + \frac{im\omega\mu}{\rho} \sum_n R_n^h(\rho) Z_n^h(z) \Phi_m^e(\phi)$$

$$E_\phi = \frac{m}{\rho} \sum_n R_n^e(\rho) Z_n^{e\prime}(z) \Phi_m^h(\phi) + i\omega\mu \sum_n R_n^{h\prime}(\rho) Z_n^h(z) \Phi_m^h(\phi)$$

$$E_z = \sum_n \lambda_{tm}^e R_n^e(\rho) Z_n^e(z) \Phi_m^e(\phi).$$

Numerical integration using the QUADPACK [19] quadrature algorithm was chosen for speed and efficiency, since the analytic integrals can become cumbersome, especially for higher order Bessel functions. For axisymmetric modes, the electric filling factors can also be calculated using the *incremental rule* [14], which is based on first order perturbation theory, taking the derivative of the resonant frequency f with respect to the permittivity of a region:

$$P_{d,p} = 2\left|\frac{\partial f}{\partial \varepsilon_p}\right|\frac{\varepsilon_p}{f}.$$

Conductor Losses

In resonator structures, conductor losses occur on metallic surfaces that have finite electrical conductivity. The losses for a particular metallic surface (labelled i) within a resonator are calculated by taking the ratio of the conductive dissipation $W_{c,i}$ per field cycle and the total stored energy U,

$$\frac{1}{Q_{c,i}} = \frac{W_{c,i}}{\omega U}.$$

The dissipation $W_{c,i}$ is found by integrating the tangential magnetic field over the conductive surface i

$$W_{c,i} = \frac{1}{2}R_{S_i}\int_{S_i}|\mathbf{H}_t|^2\mathrm{d}S.$$

The surface resistance R_{S_i} is given by

$$R_{S_i} = (f\mu_0\pi\rho_i)^{\frac{1}{2}},$$

where f is the resonant frequency and ρ_i is the resistivity of the metallic surface. The total stored magnetic energy can be calculated similarly to the previously calculated electric energy. The magnetic energy at resonance

$$U = \frac{1}{2}\mu_0\int_V \mathbf{H}\cdot\mathbf{H}^*\mathrm{d}V,$$

is equal to the electric energy, hence the loss is then:

$$\frac{1}{Q_{c,i}} = \frac{W_{c,i}}{\omega U} = \frac{R_{S_i}\int_{S_i}|\mathbf{H}_t|^2\mathrm{d}S}{\omega\mu_0\int_V \mathbf{H}\cdot\mathbf{H}^*\mathrm{d}V} = \frac{R_{S_i}}{G},$$

which introduces the *geometric factor* G, for a surface i

$$G_i = \omega\mu_0\frac{\int_V \mathbf{H}\cdot\mathbf{H}^*\mathrm{d}V}{\int_{S_i}|\mathbf{H}_t|^2\mathrm{d}S}.$$

The geometric factor G can be computed in a similar way to the incremental rule by perturbing the dimensions of the cavity:

$$G_i = \frac{\omega^2 \mu_0}{2} \left| \frac{\Delta x}{\Delta \omega} \right|$$

where Δx is a change in one of the cavity dimensions, such as diameter or height.

2.8 Example Resonator

A computer programme was written in the C++ programming language, implementing the radial mode matching technique for uniaxially anisotropic dielectric resonators. An example resonator was modelled to test the radial mode matching method and confirm its accuracy and efficiency. The resonator consisted of a $\varepsilon_r = 10$ dielectric puck with diameter 8.0 mm and height 4.0 mm placed upon a single crystal quartz support of $\varepsilon_t = 4.43$, having diameter 4.0 mm and height 4.0 mm within a silver-plated conducting cavity with diameter 20.0 mm and height 12.0 mm. The number of eigenmodes in the field expansion was increased until a convergence of less than 0.001 MHz was achieved. Figure 2.9 shows the resonant frequency convergence as the number of eigenmodes is increased. Above fifteen modes, the convergence is less than 0.01 MHz and the $TE_{01\delta}$ mode resonance had a frequency of 12.0101 GHz.

Electric filling factors for the dielectric puck and support were calculated to be 0.8929 and 0.0075, meaning 89.3 % of the electric energy resided in the puck and 0.75 % in the support. Geometric factors for the conducting cavity side, bottom and top walls were 6337, 7584 and 8171 Ω respectively, yielding an overall geometric factor of 2427 Ω. Modal field patterns for this resonance are shown in Fig. 2.10.

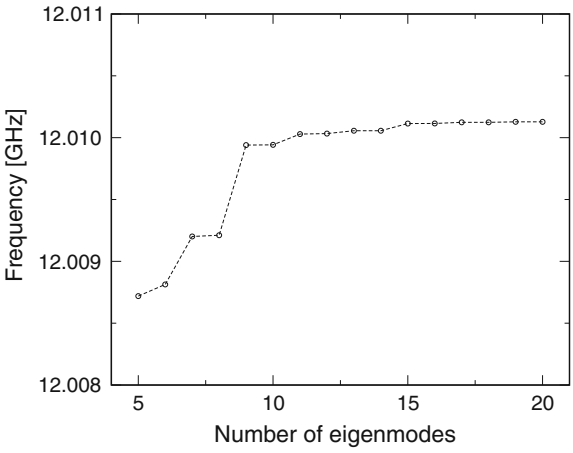

Fig. 2.9 Convergence of $TE_{01\delta}$ mode resonant frequency as a function of number of eigenmodes. Fifteen or more eigenmodes provides convergence of the resonant frequency of less than 0.01 MHz. The resonant frequency is 12.0101 GHz

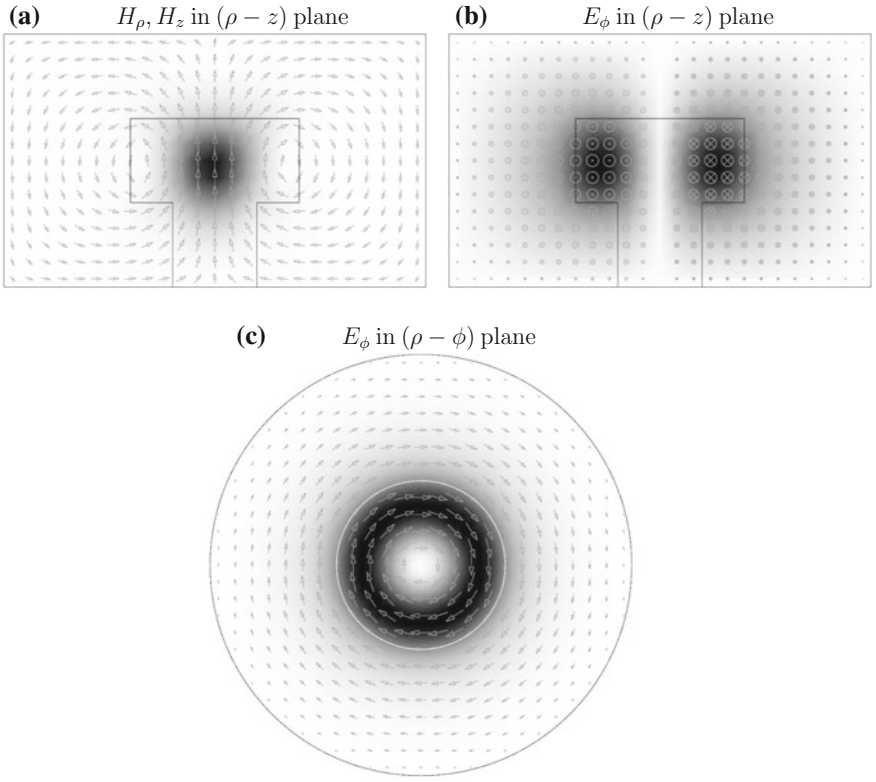

Fig. 2.10 Vector field and magnitude plots of magnetic and electric fields for a $TE_{01\delta}$ mode resonator consisting of a $\varepsilon_r = 10$ dielectric resonator of diameter 8.0 mm and height 4.0 mm placed upon a single crystal quartz support ($\varepsilon_t = 4.43$, diameter 4.0 mm and height 4.0 mm). The conducting cavity has diameter 20.0 mm and height 12.0 mm. Fifteen eigenmodes were used in the expansion of the fields resulting in a solution at 12.0101 GHz with less than 0.01 MHz convergence

2.9 Summary and Conclusions

The various types of resonator for measuring the dielectric properties of microwave ceramics were reviewed. The shielded dielectric resonator was discussed in more detail and then modelled analytically using Maxwell's equations. The radial mode matching method was implemented successfully and then used to model an example dielectric resonator, which demonstrated the efficiency and accuracy of the method.

References

1. M.E. Tobar et al., Anisotropic complex permittivity measurements of mono-crystalline rutile between 10 and 300 K. J. Appl. Phys. **83**, 1604 (1998)
2. N. Alford, M. Sebastian, A.K. Axelsson, Properties of microwave dielectric resonator materials. http://www3.imperial.ac.uk/thinfilms/dielectricproperties
3. B.W. Hakki, P.D. Coleman, A dielectric resonator method of measuring inductive capacities in the millimeter range. IEEE Trans. Microw. Theory Tech. **8**, 402 (1960)
4. W.E. Courtney, Analysis and evaluation of a method of measuring the complex permittivity and permeability of microwave insulators. IEEE Trans. Microw. Theory Tech. **18**, 476 (1970)
5. Y. Kobayashi, S. Tanaka, Resonant modes of a dielectric rod resonator short-circuited at both ends by parallel conducting plates. IEEE Trans. Microw. Theory Tech. **28**, 1077 (1980)
6. Y. Kobayashi, M. Katoh, Microwave measurement of dielectric properties of low-loss materials by the dielectric rod resonator method. IEEE Trans. Microw. Theory Tech. **33**, 586 (1985)
7. J. DelaBalle, P. Guillon, Y. Garault, Local complex permittivity measurement of MIC substrates. Int. J. Electron. Commun. **35**, 80 (1981)
8. U.S. Hong, R.H. Jansen, Numerical analysis of shielded dielectric resonators including substrate, support disc and tuning post. Electron. Lett. **18**, 1000 (1982)
9. K.A. Zaki, C. Chen, New results in dielectric-loaded resonators. IEEE Trans. Microw. Theory Tech. **34**, 815 (1986)
10. J. Krupka, Resonant modes in shielded cylindrical ferrite and single crystal dielectric resonators. IEEE Trans. Microw. Theory Tech. **37**, 691 (1989)
11. M.E. Tobar, A.G. Mann, Resonant frequencies of higher order modes in cylindrical anisotropic dielectric resonators. IEEE Trans. Microw. Theory Tech. **39**, 2077 (1991)
12. Y. Kobayashi, T. Senju, Resonant modes in shielded uniaxial-anisotropic dielectric rod resonators. IEEE Trans. Microw. Theory Tech. **41**, 2198 (1993)
13. J. Krupka et al., Complex permittivity of some ultralow loss dielectric crystals at cryogenic temperatures. Meas. Sci. Technol. **10**, 387 (1999)
14. D. Kajfez, P. Guillon, *Dielectric Resonators*, 1st edn. (Artech House, Inc., Dedham, 1964)
15. M. Abramovitz, I.A. Stegun, *Handbook of Mathematical Functions*, 9th edn. (Dover, New York, 1972)
16. S.D. Conte, C. DeBoor, *Elementary Numerical Analysis: An Algorithmic Approach*, 2nd edn. (McGraw-Hill, New York, 1965)
17. C.J.F. Ridders, Three-point iterations derived from exponential curve fitting. IEEE Trans. Circuits Syst. **26**, 669 (1979)
18. R.P. Brent, *Algorithms for Minimization without Derivatives* (Prentice-Hall, Englewood Cliffs, 1973) (Chap. 4)
19. R. Piessens et al., *QUADPACK, A Subroutine Package for Automatic Integration* (Springer, Berlin, 1983)

http://www.springer.com/978-3-319-44545-8

Temperature and Frequency Dependence of Complex Permittivity in Metal Oxide Dielectrics: Theory, Modelling and Measurement

Breeze, J.

2016, XX, 167 p. 78 illus., 27 illus. in color., Hardcover
ISBN: 978-3-319-44545-8